Nonlinear Split-Window Algorithms for Estimating Land and Sea Surface Temperatures From Simulated Chinese Gaofen-5 Satellite Data

Bo-Hui Tang, *Senior Member, IEEE*

***Abstract*— This paper proposes a different thermal channel combination split-window (DTCC-SW) method to estimate the land surface temperature (LST) and sea ST (SST) from the Chinese Gaofen-5 (GF-5) satellite thermal infrared (TIR) data. A nonlinear combination of two adjacent channels $CH_{8.20}$ (centered at 8.20 μm) and $CH_{8.63}$ (centered at 8.63 μm) was proposed to estimate LST for low-emissivity surfaces. A nonlinear combination of two adjacent channels, $CH_{10.80}$ (centered at 10.80 μm) and $CH_{11.95}$ (centered at 11.92 μm), was developed to estimate LST and SST for high-emissivity surfaces under dry atmospheric conditions, and a nonlinear combination of two channels, $CH_{8.63}$ and $CH_{11.95}$, was used to estimate LST and SST for high-emissivity surfaces under wet atmospheric conditions. The numerical values of the DTCC-SW coefficients were obtained using a statistical regression method from synthetic data simulated with an accurate atmospheric radiative transfer model moderate spectral resolution atmospheric transmittance mode 5 over a wide range of atmospheric and surface conditions. The LST (SST), mean emissivity, and atmospheric water vapor content were divided into several tractable subranges to improve the fitting accuracy. The experimental results and the preliminary evaluation results showed that the root-mean-square error between the actual and estimated LSTs (SSTs) is less than 0.7 K (0.3 K), provided that the land surface emissivities are known, which indicates that the proposed DTCC-SW method can accurately estimate the LST and SST from the GF-5 TIR data.**

***Index Terms*— Different thermal channel combination split-window (DTCC-SW), Gaofen-5 (GF-5), land surface temperature (LST), sea surface temperature (SST), thermal infrared (TIR).**

I. Introduction

SURFACE temperature (ST) is a critical parameter in the physical processes of the earth's surface energy budget and water cycle from local to global scales [1], [2]. Knowledge of the sea ST (SST) and land ST (LST) provides information on the temporal and spatial variations of the surface equilibrium state and is of fundamental importance in many applications, such as oceanography, global climate studies, geology, hydrology, and vegetation monitoring [3]–[7]. It is, consequently, crucial to have access to reliable estimates of SST and LST over large spatial and temporal scales, such as satellite observations in the thermal infrared (TIR) channels [8]–[10].

Estimations of SST and LST from satellite TIR data have been ongoing for several decades, and a large number of methods have been proposed. Based on differential water vapor absorption in two adjacent TIR channels at 11 and 12 μm, McMillin [11] first proposed the so-called split-window (SW) technique to estimate SST from satellite measurements without any information about atmospheric profiles. Since then, a variety of SW algorithms have been developed and modified to successfully estimate SST [8], [12]–[15]. Encouraged by the success of the SW technique, many efforts have been made to extend the SW technique to estimate the LST since the late 1980s. To date, various SW algorithms have been developed for estimating the LST from multispectral data observed by sensors onboard different polar-orbiting satellites and geostationary satellites [16]–[24]. Li *et al.* [9] insightfully reviewed the current algorithms and grouped the different SW algorithms into two categories, including a linear SW algorithm and a nonlinear SW algorithm, providing that the land surface emissivities (LSEs) in both the SW channels are known *a priori*. The linear SW algorithm expressed the LST as a simple linear combination of the top of atmosphere (TOA) brightness temperatures of two adjacent channels. The nonlinear SW algorithm was developed by adding a quadratic term of the difference between brightness temperatures in two adjacent channels to improve the LST retrieval accuracy for wet and hot atmospheric conditions. More detailed information is reported in [9].

The Gaofen-5 (GF-5), a polar-orbiting satellite of a series of China High-resolution Earth Observation System (CHEOS) satellites of the China National Space Administration, is scheduled to launch in 2018. It is configured with six payloads, including a visible (VIS) and shortwave infrared hyperspectral camera, a multiple spectral imager (MSI), greenhouse gas detector, an atmospheric environment infrared detector at very high spectral resolution, a differential absorption spectrometer for atmospheric trace gases, and a multiangle polarization detector. The mission of MSI is to collect land information at high spatial resolution for disaster monitoring. The MSI has a narrow swath (approximately 60 km) and observes the

Manuscript received February 9, 2018; revised April 18, 2018; accepted May 2, 2018. Date of publication May 30, 2018; date of current version October 25, 2018. This work was supported in part by the National Natural Science Foundation of China under Grant 41571353, in part by the Innovation Project of LREIS under Grant O88RA801YA, and in part by the National Key Research and Development Program of China under Grant 2016YFA0600103.

The author is with the State Key Laboratory of Resources and Environmental Information System, Institute of Geographic Sciences and Natural Resources Research, Chinese Academy of Sciences, Beijing 100101, China, and also with the College of Resources and Environment, University of Chinese Academy of Sciences, Beijing 100049, China (e-mail: tangbh@igsnrr.ac.cn).

Color versions of one or more of the figures in this paper are available online at http://ieeexplore.ieee.org.

Digital Object Identifier 10.1109/TGRS.2018.2833859

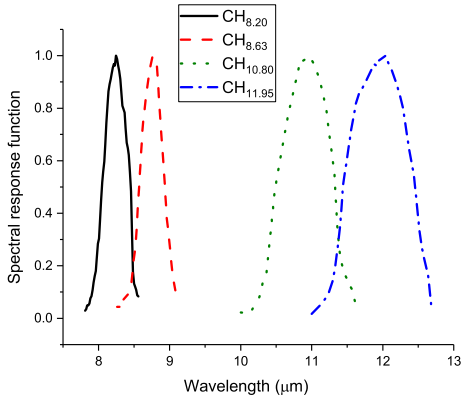

Fig. 1. Spectral response functions of four GF-5 TIR channels.

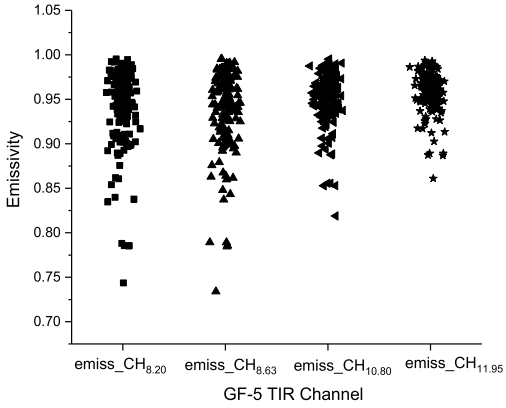

Fig. 2. Channel effective emissivities of four GF-5 TIR channels.

earth almost at nadir. It provides 13 channels that cover the spectral range from VIS/near infrared (20-m spatial resolution) to TIR (40-m spatial resolution), in which four TIR channels are centered at 8.20 ($CH_{8.20}$), 8.63 ($CH_{8.63}$), 10.80 ($CH_{10.80}$), and 11.95 μm ($CH_{11.95}$). Fig. 1 shows the spectral response functions of the four TIR channels.

Currently, two algorithms reported in the literature have been proposed to retrieve LST from the GF-5 TIR data [25], [26]. Ye *et al.* [25] proposed a four-channel algorithm to estimate the LST. The algorithm needs four channel emissivities, four channel TOA brightness temperatures, and the atmospheric water vapor content (WVC) as model inputs. Note that more input parameters needed in a model will reduce the robustness of the model. It is well known that accurately determining the channel emissivity at the pixel scale from satellite data is still problematic. The uncertainties of the four-channel emissivities and WVC will decrease the LST retrieval accuracy. In addition, the instrument noises that accompany the four TIR channels will further enlarge the LST retrieval error. Chen *et al.* [26] proposed a quadratic SW equation to retrieve LST in which the constant was parameterized as functions of the WVC, the channel mean emissivity, and the channel emissivity difference for WVC less than 1 g/cm^2 and WVC larger than 1 g/cm^2. As the authors expected, the proposed method was very sensitive to instrument noise. Assuming instrument noise of 0.2 K, 20% uncertainty in WVC and 1% uncertainty in the channel mean emissivity and the channel emissivity difference, the LST retrieval error reached 1.29 K. In addition, more than 10% of the errors between the actual and the estimated LSTs using the proposed method were larger (or less) than ± 1 K, with a maximum difference larger than 5 K or lower than -5 K.

Actually, the GF-5 satellite data have four TIR channels and meet the requirements of the temperature and emissivity separation (TES) method that can simultaneously retrieve LST and LSE [20]. However, the TES method requires synchronous atmospheric profiles to accurately correct the atmospheric effect. Otherwise, inaccurate atmospheric corrections may produce LST retrieval errors of 2–4 K for bare soil [27]. In addition, it exhibited significant errors in the estimates of LSTs and LSEs for surfaces with low spectral contrast emissivity (e.g., vegetation, water, and snow/ice) and under hot and wet atmospheric conditions [28], [29].

The objective of this paper is to develop practical SW algorithms for estimating LST and SST from the GF-5 MSI TIR data. Section II introduces the data that are used in this paper. Section III describes the development of the method to estimate LST and SST from the simulated GF-5 TIR data. The resultant LST and SST are presented in Section IV, where the sensitivity analyses in terms of the instrument noise, the uncertainty in the LSEs, and atmospheric WVC are given. Section V provides preliminary evaluations with some independent simulated GF-5 TIR data. Finally, the conclusion is drawn in Section VI.

II. Data

A. Spectral Library Data

Two spectral databases, one from the Moderate Resolution Imaging Spectroradiometer (MODIS) University of California at Santa Barbara (UCSB) emissivity library of the MODIS LST group (http://www.icess.ucsb.edu/modis/EMIS/html/em.html) and the other from Johns Hopkins University (JHU) (http://speclib.jpl.nasa.gov/), are used. The library includes spectra of rocks, minerals, lunar soils, terrestrial soils, man-made materials, meteorites, vegetation, and snow and ice covering the VIS through TIR wavelength region (0.4–14.0 μm). In total, 160 emissivity spectra consisting of 109 soil/rock types, 31 vegetation types, 10 water types, and 10 snow/ice types are used in this paper. The emissivity spectra are convolved with the spectral response functions of four GF-5 TIR channels to obtain channel effective emissivities, respectively. Fig. 2 depicts the corresponding channel effective emissivities of four GF-5 TIR channels. The emissivity values in channel $CH_{8.20}$ range from 0.744 to 0.995, from 0.734 to 0.995 for channel $CH_{8.63}$, from 0.819 to 0.995 for channel $CH_{10.80}$, and from 0.861 to 0.994 for channel $CH_{11.95}$.

B. Atmospheric Profile Data

The latest version of the Thermodynamic Initial Guess Retrieval (TIGR) database TIGR2002, constructed by the Laboratoire de Meteorologie Dynamique and representing a worldwide set of atmospheric situations (2311 radisoundings) from polar to tropical atmospheres with varying water vapor amounts ranging from 0.1 to 8 g/cm^2, is used for developing

the ST retrieval algorithm. Taking into account that the ST retrieval only considers atmospheric variation in clear-sky conditions, the profiles with relative humidity of one layer greater than 90% or two consecutive layers greater than 85% in TIGR2002 are discarded as this seldom happens under clear-sky conditions. In addition, the profiles with relative humidity at one layer within the first 2 km near the surface greater than 80% are also discarded because such skies are usually foggy. In total, 948 representative atmospheric situations are used, consisting of 813 profiles with the atmospheric WVC in [0, 2.5] g/cm^2, 60 profiles with WVC in [2.5, 3.5] g/cm^2, 49 profiles with WVC in [3.5, 4.5] g/cm^2, 26 profiles with WVC in [4.5, 6.5] g/cm^2, and the air temperatures at the bottom boundary vary from 231.25 to 314.16 K.

The six standard atmospheric profiles (tropical, midlatitude summer, midlatitude winter, subarctic summer, subarctic winter, and US76) stored in the latest atmospheric radiative transfer model moderate spectral resolution atmospheric transmittance mode (MODTRAN 5) [30] are used to evaluate the proposed LST and SST retrieval algorithms in this paper.

C. Simulated GF-5 Data

On the basis of the radiative transfer theory, for a cloud-free atmosphere under thermodynamic equilibrium, the channel radiance measured at the TOA in a TIR channel of the sensor is given with a good approximation as [31]

$$B_i(T_i) = \varepsilon_i B_i(T_s)\tau_i + R^{\uparrow}_{atm\_i} + (1-\varepsilon_i)R^{\downarrow}_{atm\_i}\tau_i \qquad (1)$$

in which T_i is the channel brightness temperature observed in channel i at the TOA, B_i is the Planck function, $B_i(T_s)$ is the radiance measured if the surface is a blackbody with ST T_s, ε_i is the channel emissivity in channel i, τ_i is the total atmospheric transmittance along the target to sensor path in channel i, $R^{\uparrow}_{\text{atm\_}i}$ is the thermal path atmospheric upwelling radiance in channel i, and $R^{\downarrow}_{\text{atm\_}i}$ is the channel downwelling atmospheric radiance in channel i.

MODTRAN5 is used with the inputs of 948 atmospheric profile data to simulate atmospheric parameters: the total spectral atmospheric transmittance τ_λ, the spectral thermal path atmospheric upwelling radiance $R^{\uparrow}_{\text{atm\_}\lambda}$, and the spectral downwelling atmospheric radiance $R^{\downarrow}_{\text{atm\_}\lambda}$. The channel atmospheric parameters (τ_i, $R^{\uparrow}_{\text{atm\_}i}$, and $R^{\downarrow}_{\text{atm\_}i}$) are determined by convolving the spectral atmospheric parameters with the spectral response functions of four GF-5 TIR channels.

To make the simulations more representative, the reasonable variations of LST are varied in a wide range according to the atmospheric temperature T_0 at the bottom boundary layer of the atmospheric profiles. That is, LST varies from $T_0 - 5$ to $T_0 + 15$ K in steps of 5 K for $T_0 \geq 290$ K, and from $T_0 - 5$ to $T_0 + 5$ K in steps of 5 K for $T_0 < 290$ K.

Then, for a given LST (T_s) in combination with the channel atmospheric parameters (τ_i, $R^{\uparrow}_{\text{atm\_}i}$, and $R^{\downarrow}_{\text{atm\_}i}$) and the channel effective emissivity ε_i mentioned earlier, the channel brightness temperature (T_i) at the TOA can be determined according to (1) with the inverse of Planck's law. In total, 517 760 different situations with T_s directly related to the TOA brightness temperatures T_i ($i = 1, \ldots, 4$) were obtained for viewing zenith angle (VZA) equivalent to 0°. Taking into account that the angular dependence of TOA radiance, an LST retrieval algorithm should account for the effect of satellite zenith angle [21], [23], [32]. However, note that the GF-5 MSI TIR sensor observes the earth's surface almost at nadir, the effect of the VZA variation on the retrieval accuracy is not considered in the development of the LST retrieval algorithm.

To simulate the GF-5 satellite data observed over the sea surface, 550 representative sea surface atmospheric profiles under cloud-free skies are extracted from TIGR2002 database. To broaden atmospheric variations to cover all possible real situations, the SST varies from $T_0 - 5$ to $T_0 + 5$ K in steps of 5 K for $T_0 \geq 290$ K, and from $T_0 - 3$ to $T_0 + 3$ K in steps of 3 K for $T_0 < 290$ K. Taking into account that the sea surface emissivities (SSEs) are basically constants for VZA less than 30° [33], [34], all seawater emissivity spectra from the JHU and UCSB databases are convolved with the spectral response functions of four GF-5 TIR channels to obtain the channel effective emissivities. Then, a mean channel emissivity is calculated for each TIR channel, i.e., 0.9817, 0.9830, 0.9866, and 0.9868 for channels $CH_{8.20}$, $CH_{8.63}$, $CH_{10.80}$, and $CH_{11.95}$, respectively. In total, 1650 different situations with SST directly related to the TOA brightness temperatures T_i ($i = 1, \ldots, 4$) are obtained for VZA = 0°.

III. Methodology

A. Development of LST Retrieval Algorithms

Wan [35] proposed a refined generalized SW (GSW) algorithm for retrieving LST (T_s) from MODIS data by adding a quadratic term of the difference between two adjacent TIR channels, written as

$$T_s = a_0 + \left(a_1 + a_2\frac{1-\bar{\varepsilon}}{\bar{\varepsilon}} + a_3\frac{\Delta\varepsilon}{\bar{\varepsilon}^2}\right)\frac{T_i + T_j}{2} + \left(a_4 + a_5\frac{1-\bar{\varepsilon}}{\bar{\varepsilon}} + a_6\frac{\Delta\varepsilon}{\bar{\varepsilon}^2}\right)\frac{T_i - T_j}{2} + a_7(T_i - T_j)^2 \qquad (2)$$

with $\bar{\varepsilon} = (\varepsilon_i + \varepsilon_j)/2$ and $\Delta\varepsilon = \varepsilon_i - \varepsilon_j$,

where T_i and T_j are the TOA brightness temperatures measured in channels i and j, respectively; ε_i and ε_j are the LSEs in channels i and j, respectively; $\bar{\varepsilon}$ is the averaged emissivity; $\Delta\varepsilon$ is the emissivity difference between the two adjacent channels; and a_k ($k = 0, 1, \ldots, 7$) are unknown coefficients.

Wan and Dozier (1996) [18] divided the averaged emissivity, atmospheric WVC, and atmospheric ST (T_0) into several subranges for improving the fitting accuracy. To make the GSW algorithm more practical, Tang *et al.* [23] proposed to use an approximate LST, replacing T_0 in the determination of the coefficients. For different values of the numerical experiments, in order to improve the accuracy of the retrieval LST, the averaged emissivities are divided into two groups: one group with averaged emissivity $\bar{\varepsilon}$ less than 0.96 (low emissivity group) and the other with $\bar{\varepsilon}$ larger than 0.94 (high emissivity group). The WVCs are divided into six subranges with an overlap of 0.5 g/cm^2: [0, 1.5], [1.0, 2.5], [2.0, 3.5], [3.0, 4.5], [4.0, 5.5], and [5.0, 6.5] g/cm^2. T_s is divided into five subranges with an

overlap of 5 K: $T_s \leq 280$, $275 \leq T_s \leq 295$, $290 \leq T_s \leq 310$, $305 \leq T_s \leq 325$, and $T_s \geq 320$ K. Then, the coefficients $a_k (k = 0, 1, \ldots, 7)$ in (2) are obtained through a statistical regressions method for each subrange.

In practice, estimating LST from the actual satellite data is conducted in two steps. First, an approximate LST is estimated using (2) with the coefficients derived for the entire range of LST, provided that the subranges of the emissivity and WVC are known; then, a more accurate LST is estimated again using (2), but with the coefficients corresponding to the tractable subrange of LST, which is determined according to the approximate LST obtained in the first step.

B. Development of SST Retrieval Algorithms

SST retrieval from the satellite TIR data was first proposed using the SW technique in the 1970s [11]. Mostly, a linear combination of two adjacent TIR channels was proposed to develop the SW algorithm. Similar to LST retrieval, to improve the retrieval accuracy of SST, particularly over hot and wet atmospheric conditions, a nonlinear SW algorithm is proposed to retrieve SST for GF-5 TIR data

$$T_s = b_0 + b_1 \frac{T_i + T_j}{2} + b_2 \frac{T_i - T_j}{2} + b_3 (T_i - T_j)^2 \quad (3)$$

where T_s represents the SST, T_i and T_j are the TOA brightness temperatures observed over the sea surface, and b_k $(k = 0, 1, \ldots, 3)$ is a set of unknown coefficients.

Similarly, the simulated GF-5 TOA brightness temperatures over sea surface are also divided into several tractable subranges for improving the fitting accuracy. Because the SSEs are assumed to be constants in this paper, the subranges are grouped as follows: 1) the WVCs are divided into four subranges with an overlap of 0.5 g/cm^2: [0, 2.0], [1.5, 3.5], [3.0, 5.0], and [4.5, 6.5] g/cm^2 and 2) T_s are divided into three subranges with an overlap of 5 K: $T_s \leq 290$, $285 \leq T_s \leq 300$, and $T_s \geq 295$ K. Then, the coefficients $b_k (k = 0, 1, \ldots, 3)$ in (3) can be obtained through a statistical regressions method for each subrange.

IV. Results and Analysis

A. Estimation and Analysis of LST

As mentioned in Section I, GF-5 MSI has four TIR channels with two groups of adjacent channels: $CH_{8.20}$ and $CH_{8.63}$ and $CH_{10.80}$ and $CH_{11.95}$. To assess the retrieval accuracy of LST estimated using the refined GSW algorithm, the LSTs are estimated separately using each combination of the four TIR channels. Fig. 3 shows the root-mean-square errors (RMSEs) between the actual and estimated LSTs for the two emissivity groups with different subranges for channel combinations of $CH_{8.20}$ and $CH_{8.63}$, $CH_{8.63}$ and $CH_{10.80}$, $CH_{8.63}$ and $CH_{11.95}$, and $CH_{10.80}$ and $CH_{11.95}$. Because the LST retrieval errors are very significant using the combinations of $CH_{8.20}$ and $CH_{10.80}$ and $CH_{8.20}$ and $CH_{11.95}$, those two combinations are not considered in this paper. Taking into account that, in reality, a lower LST is usually accompanied by less WVC, for LST less than 280 K, the maximum WVC is less than 5.5 g/cm^2. As such, there are 58 tractable subranges used in this paper. As shown in Fig. 3, the numbered subranges below 29 belong to the low emissivity group, and the others belong to the high emissivity group.

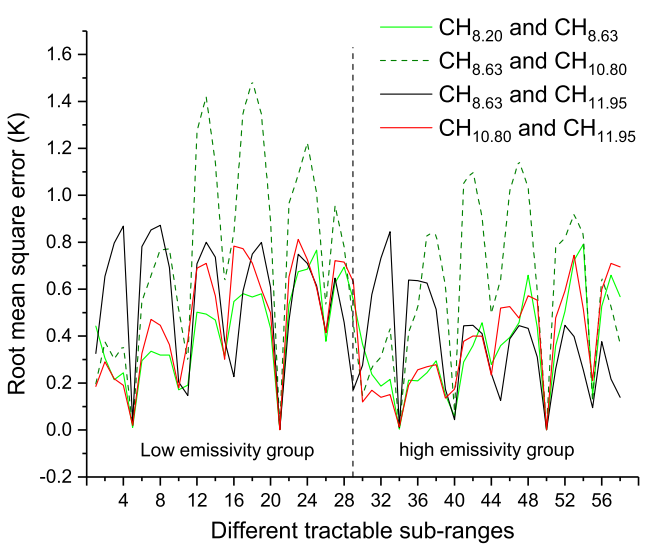

Fig. 3. RMSEs between the actual and estimated LSTs for different tractable subranges with different channel combinations of four GF-5 TIR channels.

From Fig. 3, it is apparent that the combination of two adjacent channels $CH_{8.20}$ and $CH_{8.63}$ is comparable with the combination of channels $CH_{10.80}$ and $CH_{11.95}$ for estimating LST using the refined GSW algorithm. All RMSEs are below 0.8 K for those two combinations. For low emissivity group, the combination of $CH_{8.20}$ and $CH_{8.63}$ is better than the combination of $CH_{10.80}$ and $CH_{11.95}$, where the RMSEs are below 0.5 K for low WVC conditions (WVC $\leq$ 3.5 g/cm^2) and are below 0.7 K for high WVC conditions (WVC $>$ 3.5 g/cm^2). In addition, it is also apparent that the combination of channels $CH_{8.63}$ and $CH_{11.95}$ can be used to retrieve LST with the GSW algorithm. Particularly, for the high emissivity group and high WVC conditions (WVC $>$ 3.5 g/cm^2), the combination of $CH_{8.63}$ and $CH_{11.95}$ retrieves LST with the lowest RMSE errors, and all RMSEs in subranges from 39 to 58 are below 0.5 K. Consequently, the combination of channels $CH_{8.20}$ and $CH_{8.63}$ is selected to retrieve LST for the low emissivity group. For the high emissivity group, the combination of channels $CH_{10.80}$ and $CH_{11.95}$ is used to retrieve LST if WVC $\leq$ 3.5 g/cm^2, and the combination of channels $CH_{8.63}$ and $CH_{11.95}$ is used to retrieve LST for WVC $>$ 3.5 g/cm^2. Hereafter, the different channel combination selections used in this paper are called the different thermal channel combination SW (DTCC-SW) method.

As an example, Fig. 4 shows the histogram of the difference between the actual T_s and those estimated using the channel combination of $CH_{8.20}$ and $CH_{8.63}$ for the low emissivity group with coefficients corresponding to the subranges WVC $\in [0, 1.5]$, $T_s \leq 280$ K, and WVC $\in [5.0, 6.5]$, $T_s \geq 320$ K, respectively. As shown in Fig. 4, the RMSE is 0.44 K for very dry and cold atmospheres, and is 0.55 K for very wet and hot atmospheres. Similar results are obtained for the other 27 subranges, and all RMSEs are below 0.7 K.

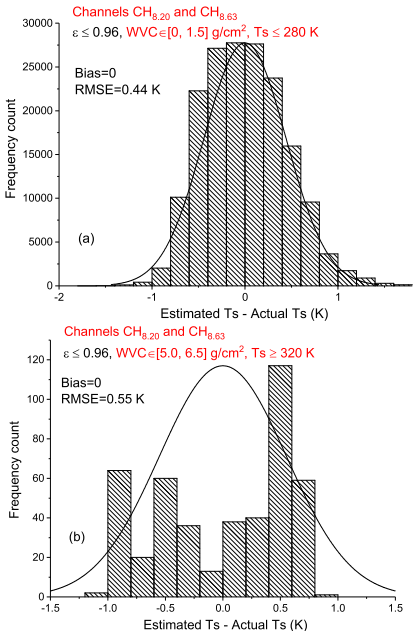

Fig. 4. Histogram of the difference between the actual T_s and those estimated using the channel combination of $CH_{8.20}$ and $CH_{8.63}$ for the low emissivity group. (a) For the subrange with WVC $\in$ [0, 1.5] and $T_s \leq 280$ K. (b) For the subrange with WVC $\in$ [5.0, 6.5] and $T_s \geq 320$ K.

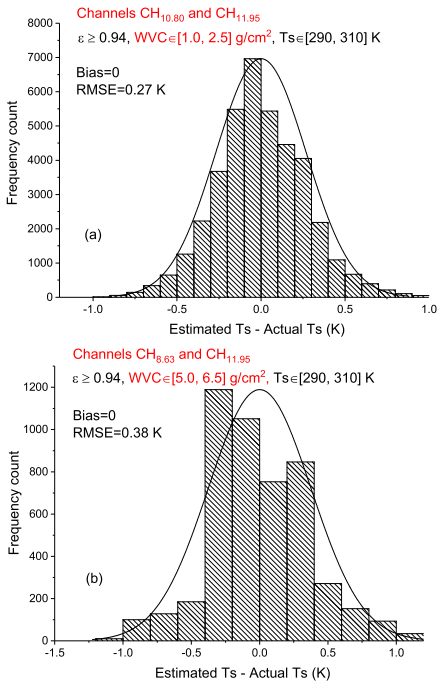

Fig. 5. Histogram of the difference between the actual and estimated T_s for the high emissivity group. (a) Using the channel combination of $CH_{10.80}$ and $CH_{11.95}$ for the subrange with WVC $\in$ [1.0, 2.5] g/cm^2 and $T_s \in$ [290, 310] K. (b) Using the channel combination of $CH_{8.63}$ and $CH_{11.95}$ for the subrange with WVC $\in$ [5.0, 6.5] g/cm^2 and $T_s \in$ [290, 310] K.

As far as the high emissivity group is concerned, Fig. 5(a) shows one histogram of the difference between the actual and the estimated T_s using the channel combination of $CH_{10.80}$ and $CH_{11.95}$ for the subrange with WVC $\in$ [1.0, 2.5] g/cm^2 and $T_s \in$ [290, 310] K. As shown in Fig. 5(a), the RMSE is 0.27 K and the maximum differences are within $\pm$1 K. Fig. 5(b) shows the histogram of the difference between the actual and the estimated T_s using the channel combination of $CH_{8.63}$ and $CH_{11.95}$ for the subrange with WVC $\in$ [5.0, 6.5] g/cm^2 and $T_s \in$ [290, 310] K. The RMSE is 0.38 K and the maximum differences are within $\pm$1.5 K. For the other 27 subranges, similar results are obtained using the two combinations, and all RMSEs are below 0.5 K.

B. Estimation and Analysis of SST

Similar to the LST retrieval, the four GF-5 TIR channels are separately combined and the SSTs are retrieved using each combination of the channels with the proposed SW algorithm of (3), respectively. Since the lower LST is very few accompanied by very high WVC, the subrange with LST less than 290 K and WVC $\in$ [4.5, 6.5] g/cm^2 is not considered. Therefore, there are 11 tractable subranges used in this paper. Fig. 6 shows the RMSEs between the actual and estimated SSTs for different tractable subranges with different channel combinations of four GF-5 TIR channels. As shown in Fig. 6, the numbered subranges 1–6 belong to the low WVC group (WVC $\leq$ 3.5 g/cm^2) and the others belong to the high WVC group (WVC $>$ 3.5 g/cm^2).

From Fig. 6, it is apparent that channels $CH_{10.80}$ and $CH_{11.95}$ constitute the best combination for estimating SST using the proposed SW algorithm with all RMSEs below 0.3 K for the low WVC group. The combination of channels $CH_{8.63}$

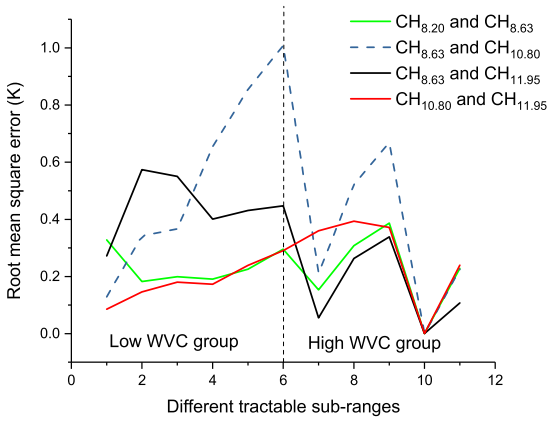

Fig. 6. RMSEs between the actual and estimated SSTs for different tractable subranges with different channel combinations of four GF-5 TIR channels.

and $CH_{11.95}$ is the best for estimating SST with all RMSEs less than 0.34 K for the high WVC group. Consequently, the combination of channels $CH_{10.80}$ and $CH_{11.95}$ is selected to retrieve SST for the low WVC group, and the combination of channels $CH_{8.63}$ and $CH_{11.95}$ is used to retrieve SST for the high WVC group in this paper.

Fig. 7(a) shows the histogram of the differences between the estimated and the actual SSTs using the channel combination of $CH_{10.80}$ and $CH_{11.95}$ for all six subranges in the low WVC group. The maximum difference is below 0.7 K and 97% of the differences are within $\pm$0.3 K. Fig. 7(b) shows the histogram of the estimated and actual SST differences for the channel combination of $CH_{8.63}$ and $CH_{11.95}$ for the other five

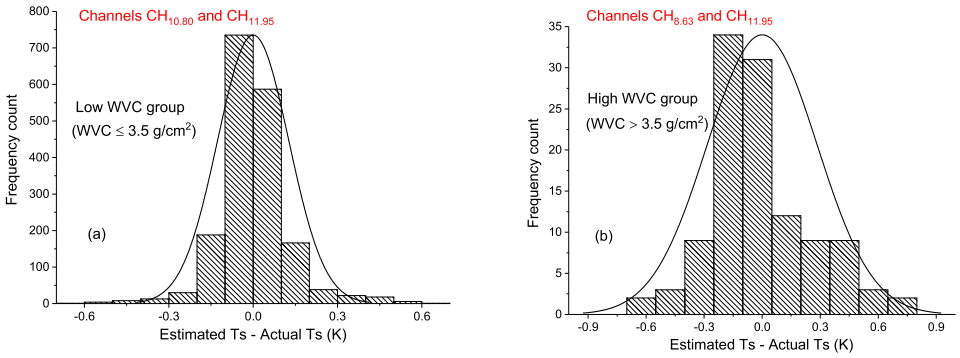

Fig. 7. Histogram of the difference between the actual and estimated SSTs for (a) using the channel combination of $CH_{10.80}$ and $CH_{11.95}$ for the low WVC group and (b) using the channel combination of $CH_{8.63}$ and $CH_{11.95}$ for the high WVC group.

TABLE I

LST RETRIEVAL ERRORS CAUSED BY INSTRUMENT NOISE (NEΔT) FOR SIX SUBRANGES WITH $\bar{\varepsilon} > 0.94$ AND $T_s \in [290, 310]$ K

WVC (g/cm^2)	LST retrieval errors (RMSEs) (K)						
	Without NEΔT	NEΔT =0.1 K	Difference to without NEΔT	NEΔT =0.2 K	Difference to without NEΔT	NEΔT =0.5 K	Difference to without NEΔT
[0.0, 1.5]	0.14	0.17	0.03	0.23	0.09	0.48	0.34
[1.0, 2.5]	0.27	0.29	0.02	0.33	0.06	0.53	0.26
[2.0, 3.5]	0.40	0.41	0.01	0.44	0.04	0.59	0.19
[3.0, 4.5]	0.44	0.46	0.02	0.49	0.05	0.68	0.24
[4.0, 5.5]	0.45	0.46	0.01	0.49	0.04	0.68	0.23
[5.0, 6.5]	0.38	0.39	0.01	0.43	0.05	0.63	0.25

TABLE II

SST RETRIEVAL ERRORS CAUSED BY INSTRUMENT NOISE (NEΔT) FOR FOUR SUBRANGES WITH DIFFERENT WVCS AND SST > 295 K

WVC (g/cm^2)	SST retrieval errors (RMSEs) (K)						
	Without NEΔT	NEΔT =0.1 K	Difference to without NEΔT	NEΔT =0.2 K	Difference to without NEΔT	NEΔT =0.5 K	Difference to without NEΔT
[0.0, 2.0]	0.18	0.21	0.03	0.26	0.08	0.49	0.31
[1.5, 3.5]	0.29	0.31	0.02	0.34	0.05	0.52	0.23
[3.0, 5.0]	0.34	0.36	0.02	0.40	0.06	0.62	0.28
[4.5, 6.5]	0.11	0.16	0.05	0.24	0.13	0.54	0.43

subranges in the high WVC group. The maximum difference is below 1.0 K and 82.6% of the differences are within ± 0.3 K.

C. Sensitivity Analysis

Three main error sources related to the instrument noise (NEΔT), the uncertainty of LSEs, and the uncertainty of WVC that influence the ST retrieval accuracy are taken into account in this investigation.

1) Instrument Noise (NEΔT): Noise-equivalent temperature differences (NEΔT) mainly come from the radiometric performance of the instrument and influences the values of the TOA brightness temperatures. The NΔT is desigated as 0.2 K for the four GF-5 MSI TIR channels. To assess the influence of the instrument NΔT on the ST retrieva, a Gaussian random distribution of noises (totally 100 numbers) with a mean of 0 K and a standard deviation of 0.1 K is added to each of the simulated GF-5 TOA brightness temperature. Then, the STs are recalculated using the proposed DTCC-SW algorithm with the noised TOA brightness temperatures. In addition, to assess the significance of the influence, an NΔT of 0.2 and 0.5 K is also investigated in this paper. As an example, Table I lists comparisons between the RMSEs of LSTs estimated using the simulated TOA brightness temperatures without NΔT and those with NΔT for the high emissivity group and LST ranging from 20 to 310 K. From Table I, it is apparent that the LST retrieval error increases as NΔ increases, and the influence of NEΔT on the LST retrieval error under dry atmospheres is greater than under wet atmospheres. The maximum of the RMSE difference is 0.34 K for WVC $\in [0.0, 1.5]$ g/cm^2 when NEΔT equals 0.5 K. However, when NEΔT equals 0.2 K, the maximum RMSE difference is 0.09 K for the subrange $\bar{\varepsilon} > 0.94$, WVC $\in [0.0, 1.5] g/cm^2$, and $T_s \in [290, 310]$ K.

In addition, to assess the influence of the instrument NEΔT on the SST retrieval, Table II depicts comparisons of the RMSEs estimated using the TOA brightness temperatures with/without NEΔT. The SST retrieval error also increases as NEΔT increases. Keep in mind that the proposed DTCC-SW

TABLE III
LST RETRIEVAL ERRORS (RMSES) CAUSED BY THE UNCERTAINTY OF LSES FOR TWELVE SUBRANGES WITH $T_s \in [290, 310]$ K

WVC (g/cm^2)	RMSEs for the low emissivity group (K)			RMSEs for the high emissivity group (K)		
	Without LSE uncertainty	With LSE uncertainty of 1%	Difference	Without LSE uncertainty	With LSE uncertainty of 1%	Difference
[0.0, 1.5]	0.21	0.25	0.04	0.14	1.50	1.36
[1.0, 2.5]	0.32	0.34	0.02	0.27	1.45	1.18
[2.0, 3.5]	0.49	0.50	0.01	0.40	1.35	0.95
[3.0, 4.5]	0.57	0.57	0.00	0.44	0.92	0.48
[4.0, 5.5]	0.67	0.68	0.01	0.45	0.80	0.35
[5.0, 6.5]	0.63	0.63	0.00	0.38	0.67	0.29

TABLE IV
LST RETRIEVAL ERRORS CAUSED BY THE UNCERTAINTY OF WVC FOR SIX SUBRANGES WITH $\bar{\varepsilon} > 0.94$ AND $T_s \in [290, 310]$ K. THE ARROW INDICATES THE RMSE CHANGE CAUSED USING INCORRECT COEFFICIENTS OF AN ADJACENT SUBRANGE

WVC (g/cm^2)	LST retrieval errors (RMSEs) (K)											
	[0.0, 1.5]		[1.0, 2.5]		[2.0, 3.5]		[3.0, 4.5]		[4.0, 5.5]		[5.0, 6.5]	
[0.0, 1.5]	**0.14**	→	0.34									
[1.0, 2.5]	0.38	←	**0.27**	→	0.74							
[2.0, 3.5]			0.69	←	**0.40**	→	0.44					
[3.0, 4.5]					0.40	←	**0.44**	→	0.67			
[4.0, 5.5]							0.65	←	**0.45**	→	0.93	
[5.0, 6.5]									0.72	←	**0.38**	

method uses the channel combination of $CH_{10.80}$ and $CH_{11.95}$ to retrieve SST for the low WVC group and the combination of $CH_{8.63}$ and $CH_{11.95}$ for the high WVC group. It is interesting that the influence of NEΔT on SST retrieval error under wet atmospheres is greater than under dry atmospheres for the high WVC group. The maximum RMSE difference is 0.43 K for the subrange WVC $\in [4.5, 6.5]$ g/cm^2 and $T_s > 295$ K. When the NEΔT equals 0.2 K, the maximum RMSE difference is 0.13 K for the subrange WVC $\in [4.5, 6.5]$ g/cm^2 and $T_s > 295$ K.

2) Uncertainty of LSEs: Considering that the SSEs are assumed to be constants in the development of the SST retrieval algorithm, only the influence of the uncertainty of LSEs on the LST retrieval is analyzed in this paper, assuming that 1% uncertainty of LSEs is added to the averaged $\bar{\varepsilon}$ and the emissivity difference $\Delta\varepsilon$. The LSTs are recalculated again using (2). Table III gives comparisons of the LST retrieval errors with/without the uncertainty of LSEs for 12 subranges with the same LST variation range $T_s \in [290, 310]$ K. As shown in Table III, the influence of LSEs uncertainty on the LST retrieval for the low emissivity group can be ignored with a maximum difference of 0.04 K. However, the influence for the high emissivity group is very significant, particularly for the dry atmospheres with a maximum difference up to 1.36 K, where the LSTs are estimated using the combination of channels $CH_{10.80}$ and $CH_{11.95}$. This indicates that the LSEs should be known in priori for accurately estimating the LST for surfaces with high emissivities under dry atmospheric conditions.

3) Uncertainty of WVC: Note that the proposed DTCC-SW method divides the WVC into six subranges with an overlap of 0.5 g/cm^2. The overlapped WVC can be divided into two adjacent subranges. Specifically, the two subranges correspond to two pairs of coefficients. As such, the effect of the uncertainty of WVC on ST retrieval is mainly due to the incorrect subrange selection of WVC. To analyze the effect of WVC overlap on ST retrieval, the STs are recalculated using the coefficients obtained for the adjacent subranges. Table IV gives the LST retrieval errors caused by using incorrect coefficients in adjacent subranges for the high emissivity group and $T_s \in [290, 310]$ K. The arrow implies that the RMSE will change when the LST is estimated using incorrect coefficients of an adjacent subrange. The results reveal that the RMSE differences range from 0.04 to 0.48 K, and the maximum occurs for the subrange WVC $\in [4.0, 5.5]$ g/cm^2 when using the coefficients from the subrange WVC $\in [5.0, 6.5]$ g/cm^2.

It should be noted here that the proposed method uses the channel combination of $CH_{10.80}$ and $CH_{11.95}$ to retrieve LST for the low WVC group and the combination of $CH_{8.63}$ and $CH_{11.95}$ for the high WVC group. No matter what the WVC overlap [3.0, 3.5] is classified as, the LST will be retrieved using the corrected coefficients of the subrange. As such, the influence of the uncertainty of WVC on the retrieval of LST is the least.

Table V gives the SST retrieval errors caused by using incorrect coefficients in adjacent subranges for $T_s > 295$ K.

TABLE V
SST RETRIEVAL ERRORS CAUSED BY THE UNCERTAINTY OF WVC FOR FOUR SUBRANGES WITH $T_s > 295$ K. THE ARROW INDICATES THE RMSE CHANGE USING INCORRECT COEFFICIENTS OF AN ADJACENT SUBRANGE

WVC (g/cm^2)	SST retrieval errors (RMSEs) (K)							
	[0.0, 2.0]		[1.5, 3.5]		[3.0, 5.5]		[4.5, 6.5]	
[0.0, 2.0]	**0.18**	→	0.30					
[1.5, 3.5]	0.43	←	**0.29**	→	0.34			
[3.0, 5.5]			0.29	←	**0.34**	→	0.83	
[4.5, 6.5]					0.47	←	**0.11**	

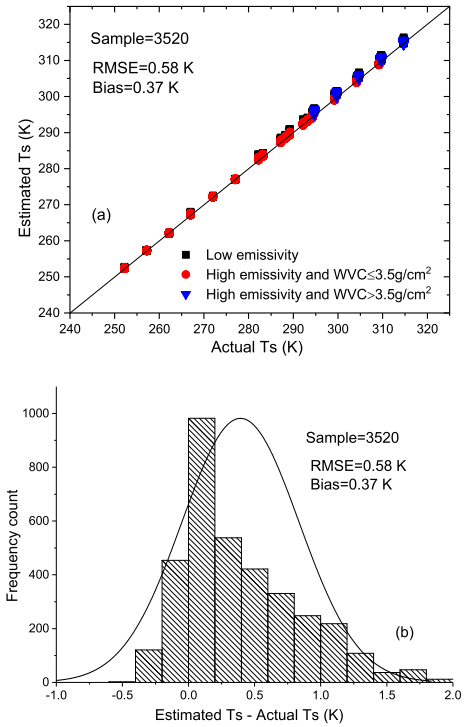

Fig. 8. (a) Comparison and (b) histogram of the difference between the actual LSTs and those estimated from independent GF-5 satellite data simulated using the six standard atmospheric profiles of MODTRAN5 and the JHU and UCSB emissivity spectra.

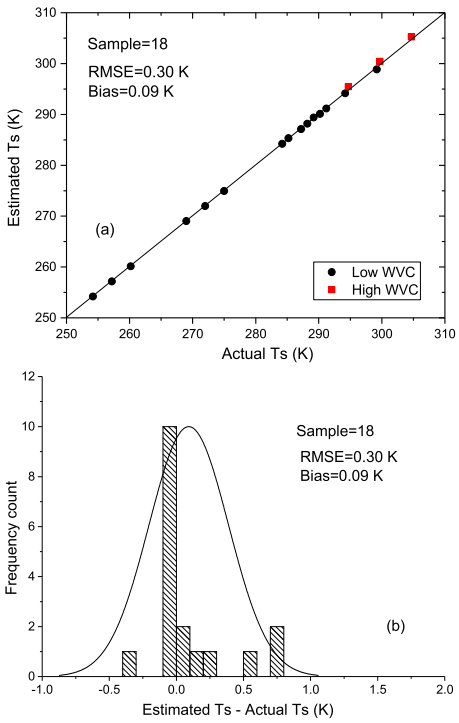

Fig. 9. (a) Comparison and (b) histogram of the difference between actual SSTs and those estimated from independent GF-5 satellite data simulated using the six standard atmospheric profiles of MODTRAN5 and the constant channel emissivities.

The results reveal that the RMSE differences vary from 0.05 to 0.49 K, and the maximum occurs for the subrange WVC $\in$ $[3.0, 5.5]$ g/cm^2 when using the coefficients of the subrange WVC $\in$ $[4.5, 6.5]$ g/cm^2.

V. Evaluations

Considering that the GF-5 satellite has not yet been launched, some independent GF-5 satellite data simulated using the six standard atmospheric profiles of MODTRAN5 and the JHU and UCSB emissivity spectra are used to preliminarily evaluate the proposed DTCC-SW algorithm. Fig. 8(a) shows a comparison of the actual LSTs and those estimated using the proposed method. The comparison results show that the LSTs are slightly overestimated when the WVC is greater than 3.5 g/cm^2 for all cases. However, overall, the bias and RMSE are 0.37 and 0.58 K, respectively. Fig. 8(b) shows the corresponding histogram of the differences between the actual and estimated LSTs. As Fig. 8 shows, the maximum difference is less than 2.0 K, and 87.6% of the differences are within $\pm$0.7 K, indicating that the proposed algorithm is appropriate for retrieving LST from the GF-5 satellite data.

In addition, the proposed SST retrieval algorithm is also evaluated using the simulated GF-5 satellite data over the sea surface. The six standard atmospheric profiles of MODTRAN5 and the constant emissivity of each channel are used for the simulations. Fig. 9(a) shows comparisons of the actual SSTs and those estimated using the proposed DTCC-SW algorithm, and Fig. 9(b) shows the corresponding histogram of the difference. As shown in Fig. 9, the proposed DTCC-SW algorithm slightly overestimates the SSTs, particularly for high WVC conditions. However, generally speaking, the retrieval accuracy is encouraging. The bias and RMSE are 0.09 and 0.30 K, respectively, which meet the requirements of the global climate change study that needs SST retrieval accuracy better than 0.3 K.

VI. Conclusion

In this paper, a DTCC-SW method is proposed to estimate ST from the CHEOS GF-5 satellite TIR data. To improve the ST retrieval accuracy, a nonlinear channel combination of $CH_{8.20}$ (centered at 8.20 μm) and $CH_{8.63}$ (centered at 8.63 μm) was proposed to estimate LST for low-emissivity surfaces; a nonlinear combination of channels $CH_{10.80}$ (centered at 10.80 μm) and $CH_{11.95}$ (centered at 11.92 μm) was developed to estimate LST and SST for high-emissivity surfaces under dry atmospheric conditions; and a nonlinear combination of channels $CH_{8.63}$ and $CH_{11.95}$ was used to estimate LST and SST for high-emissivity surfaces under wet atmospheric conditions.

On the basis of a radiative transfer theory, the proposed DTCC-SW algorithm was developed using an accurate atmospheric radiative transfer model MODTRAN5 with inputs of the TIGR atmospheric profile database and the JHU and UCSB spectral databases. The coefficients in the DTCC-SW algorithm were derived using a statistical regression method from numerically simulated GF-5 TIR data, which were divided into several tractable subranges according to the ranges of the mean emissivity, WVC, and ST.

Sensitivity analyses related to instrument noise, the uncertainty in the LSEs, and atmospheric WVC were performed. The results showed that the ST retrieval errors increased as NEΔT increased. The influence of NEΔT on the LST retrieval errors under dry atmospheres was larger than under wet atmospheres, whereas the opposite result was obtained for SST retrieval errors. Compared to LST retrieval without NEΔT, adding NEΔT of 0.2 K resulted in a maximum RMSE difference of 0.09 K, as well as 0.13 K for the SST retrieval. Assuming that 1% uncertainty of LSEs was added to the averaged $\bar{\varepsilon}$ and the emissivity difference $\Delta\varepsilon$, the influence on the LST retrieval error could be ignored for the low emissivity group with a maximum RMSE difference of 0.04 K. However, the influence for the high emissivity group was very significant, particularly for the dry atmospheres with a maximum RMSE difference up to 1.36 K. The uncertainty of WVC could cause the LST retrieval errors of the RMSE differences that ranged from 0.04 to 0.48 K, and from 0.05 to 0.49 K for SST retrieval errors.

The experimental results showed that the RMSE between the actual LSTs and those estimated using the proposed DTCC-SW algorithm for low emissivity group was 0.44 K under very dry and cold atmospheres, and 0.55 K for very wet and hot atmospheres. For the high emissivity group, the maximum RMSE was below 0.5 K. For SST retrieval, the maximum RMSE was less than 0.3 K for the low WVC group, and was 0.34 K for the high WVC group. Preliminary evaluations with some independently simulated GF-5 TIR data demonstrated that the bias and RMSE between the actual and estimated LSTs were 0.37 and 0.58 K, respectively, and those for SST were 0.09 and 0.30 K, respectively. Generally, the proposed DTCC-SW method is appropriate for estimating ST from the GF-5 satellite data, with an accuracy of 0.7 K for LST retrieval and an accuracy of 0.3 K for SST retrieval.

REFERENCES

[1] A. Karnieli *et al.*, "Use of NDVI and land surface temperature for drought assessment: Merits and limitations," *J. Climate*, vol. 23, pp. 618–633, Feb. 2010.

[2] W. Kustas and M. Anderson, "Advances in thermal infrared remote sensing for land surface modeling," *Agricult. Forest Meteorol.*, vol. 149, pp. 2071–2081, Dec. 2009.

[3] H. Mannstein, "Surface energy budget, surface temperature and thermal inertia," in *Remote Sensing Applications in Meteorology and Climatology* (NATO ASI Series), vol. 201, R. A. Vaughan and D. Reidel, Eds. Dordrecht, The Netherlands: Springer-Verlag, 1987.

[4] Z.-L. Li *et al.*, "A review of current methodologies for regional evapotranspiration estimation from remotely sensed data," *Sensors*, vol. 9, no. 5, pp. 3801–3853, 2009.

[5] Q. Weng, "Thermal infrared remote sensing for urban climate and environmental studies: Methods, applications, and trends," *ISPRS J. Photogramm. Remote Sens.*, vol. 64, pp. 335–344, Jul. 2009.

[6] F. N. Kogan, "Operational space technology for global vegetation assessment," *Bull. Amer. Meteorol. Soc.*, vol. 82, pp. 1949–1964, Sep. 2001.

[7] Y. H. Kerr, J. P. Lagouarde, F. Nerry, and C. Ottle, "Land surface temperature retrieval techniques and applications," in *Thermal Remote Sensing in Land Surface Processing*, D. A. Quattrochi and J. C. Luvall, Eds. Boca Raton, FL, USA: CRC Press, 2000, pp. 33–109.

[8] J. A. Sobrino, Z.-L. Li, M. P. Stoll, and F. Becker, "Multi-channel and multi-angle algorithms for estimating sea and land surface temperature with ATSR data," *Int. J. Remote Sens.*, vol. 17, no. 11, pp. 2089–2114, 1996.

[9] Z.-L. Li *et al.*, "Satellite-derived land surface temperature: Current status and perspectives," *Remote Sens. Environ.*, vol. 131, pp. 14–37, Apr. 2013.

[10] Z.-L. Li *et al.*, "Land surface emissivity retrieval from satellite data," *Int. J. Remote Sens.*, vol. 34, nos. 9–10, pp. 3084–3127, 2013.

[11] L. M. McMillin, "Estimation of sea surface temperatures from two infrared window measurements with different absorption," *J. Geophys. Res.*, vol. 80, pp. 5113–5117, Dec. 1975.

[12] P. Y. Deschamps and T. Phulpin, "Atmospheric correction of infrared measurements of sea surface temperature using channels at 3.7, 11 and 12 μm," *Boundary Layer Meteorol.*, vol. 18, no. 2, pp. 131–143, 1980.

[13] J. A. Sobrino, V. Caselles, and C. Coll, "Theoretical split-window algorithms for determining the actual surface temperature," *IL Nuovo Cimento C*, vol. 16, pp. 219–236, May 1993.

[14] G. B. França and W. S. Carvalho, "Sea surface temperature GOES-8 estimation approach for the Brazilian coast," *Int. J. Remote Sens.*, vol. 25, no. 17, pp. 3439–3450, 2004.

[15] R. Niclòs, V. Caselles, C. Coll, and E. Valor, "Determination of sea surface temperature at large observation angles using an angular and emissivity-dependent split-window equation," *Remote Sens. Environ.*, vol. 111, pp. 107–121, Nov. 2007.

[16] F. Becker and Z.-L. Li, "Towards a local split window method over land surfaces," *Int. J. Remote Sens.*, vol. 11, no. 11, pp. 369–393, 1990.

[17] Z.-L. Li and F. Becker, "Feasibility of land surface temperature and emissivity determination from AVHRR data," *Remote Sens. Environ.*, vol. 43, pp. 67–85, Jan. 1993.

[18] Z. Wan and J. Dozier, "A generalized split-window algorithm for retrieving land-surface temperature from space," *IEEE Trans. Geosci. Remote Sens.*, vol. 34, no. 4, pp. 892–905, Jul. 1996.

[19] Z. Wan and Z.-L. Li, "A physics-based algorithm for retrieving land-surface emissivity and temperature from EOS/MODIS data," *IEEE Trans. Geosci. Remote Sens.*, vol. 35, no. 4, pp. 980–996, Jul. 1997.

[20] A. Gillespie *et al.*, "A temperature and emissivity separation algorithm for advanced spaceborne thermal emission and reflection radiometer (ASTER) images," *IEEE Trans. Geosci. Remote Sens.*, vol. 36, no. 4, pp. 1113–1126, Apr. 1998.

[21] B.-H. Tang, K. Shao, Z.-L. Li, H. Wu, F. Nerry, and G. Zhou, "Estimation and validation of land surface temperatures from Chinese second-generation polar-orbit FY-3A VIRR data," *Remote Sens.*, vol. 7, no. 3, pp. 3250–3273, 2015.

[22] J. A. Sobrino and M. Romaguera, "Land surface temperature retrieval from MSG1-SEVIRI data," *Remote Sens. Environ.*, vol. 92, no. 2, pp. 247–254, 2004.

[23] B.-H. Tang *et al.*, "Generalized split-window algorithm for estimate of land surface temperature from Chinese geostationary FengYun meteorological satellite (FY-2C) data," *Sensors*, vol. 8, pp. 933–951, Sep. 2008.

[24] G.-M. Jiang and R. Liu, "Retrieval of sea and land surface temperature from SVISSR/FY-2C/D/E measurements," *IEEE Trans. Geosci. Remote Sens.*, vol. 52, no. 10, pp. 6132–6140, Oct. 2014.

[25] X. Ye, H. Ren, R. Liu, Q. Qin, Y. Liu, and J. Dong, "Land surface temperature estimate from Chinese Gaofen-5 satellite data using split-window algorithm," *IEEE Trans. Geosci. Remote Sens.*, vol. 55, no. 10, pp. 5877–5888, Oct. 2017.

[26] Y. Chen, S.-B. Duan, H. Ren, J. Labed, and Z.-L. Li, "Algorithm development for land surface temperature retrieval: Application to Chinese Gaofen-5 data," *Remote Sens.*, vol. 9, no. 2, p. 161, 2017.

[27] P. Dash, F.-M. Göttsche, F.-S. Olesen, and H. Fischer, "Land surface temperature and emissivity estimation from passive sensor data: Theory and practice-current trends," *Int. J. Remote Sens.*, vol. 23, no. 3, pp. 2563–2594, 2002.

[28] A. R. Gillespie, E. A. Abbott, L. Gilson, G. Hulley, J. C. Jiménez-Muñoz, and J. A. Sobrino, "Residual errors in ASTER temperature and emissivity standard products AST08 and AST05," *Remote Sens. Environ.*, vol. 115, pp. 3681–3694, Dec. 2011.

[29] G. C. Hulley and S. J. Hook, "Generating consistent land surface temperature and emissivity products between ASTER and MODIS data for earth science research," *IEEE Trans. Geosci. Remote Sens.*, vol. 49, no. 4, pp. 1304–1315, Apr. 2011.

[30] A. Berk *et al.*, "MODTRAN cloud and multiple scattering upgrades with application to AVIRIS," *Remote Sens. Environ.*, vol. 65, pp. 367–375, Sep. 1998.

[31] Z. Li, F. Petitcolin, and R. Zhang, "A physically based algorithm for land surface emissivity retrieval from combined mid-infrared and thermal infrared data," *Sci. China E, Technol. Sci.*, vol. 43, pp. 23–33, Dec. 2000.
[32] D. Sun and R. T. Pinker, "Estimation of land surface temperature from a Geostationary Operational Environmental Satellite (GOES-8)," *J. Geophys. Res.*, vol. 108, no. D11, Jun. 2003, Art. no. 4326.
[33] K. Masuda, T. Takashima, and Y. Takayama, "Emissivity of pure and sea waters for the model sea surface in the infrared window regions," *Remote Sens. Environ.*, vol. 24, no. 2, pp. 313–329, Mar. 1988.
[34] X. Wu and W. L. Smith, "Emissivity of rough sea surface for 8–13 μm: Modeling and verification," *Appl. Opt.*, vol. 36, no. 12, pp. 2609–2619, 1997.
[35] Z. Wan, "New refinements and validation of the collection-6 MODIS land-surface temperature/emissivity product," *Remote Sens. Environ.*, vol. 140, pp. 36–45, Jan. 2014.

Bo-Hui Tang (SM'11) received the B.S. degree in cartography and geographical information system from Wuhan University, Wuhan, China, in 1999, the M.S. degree in cartography and geographical information system from China Remote Sensing Satellite Ground Station, Chinese Academy of Sciences, Beijing, China, in 2004, and the Ph.D. degree in cartography and geographical information system from the Institute of Geographic Sciences and Natural Resources Research, Chinese Academy of Sciences, in 2007.

He is currently an Associate Research Fellow with the Institute of Geographic Sciences and Natural Resources Research. His research interests include the retrieval and validation of surface net radiation and surface temperature.